

Evolution of the magnetorotational instability on initially tangled magnetic fields

Pallavi Bhat,^{1,2}★ Fatima Ebrahimi,¹ Eric G. Blackman,³ and Kandaswamy Subramanian,⁴

¹*Department of Astrophysical Sciences and Princeton Plasma Physics Laboratory, Princeton University, Princeton, NJ 08543, USA*

²*Plasma Science and Fusion Center, Massachusetts Institute of Technology, Cambridge, MA 02139, USA*

³*Department of Physics and Astronomy, University of Rochester, Rochester, NY 14618, USA*

⁴*Inter University Centre for Astronomy and Astrophysics, Post Bag 4, Pune University Campus, Ganeshkhind, Pune 411 007, India*

Accepted XXX. Received YYY; in original form ZZZ

ABSTRACT

The initial magnetic field of previous magnetorotational instability (MRI) simulations has always included a significant system-scale component, even if stochastic. However, it is of conceptual and practical interest to assess whether the MRI can grow when the initial field is turbulent. The ubiquitous presence of turbulent or random flows in astrophysical plasmas generically leads to a small-scale dynamo (SSD), which would provide initial seed turbulent velocity and magnetic fields in the plasma that becomes an accretion disc. Can the MRI grow from these more realistic initial conditions? To address this we supply a standard shearing box with isotropically forced SSD generated magnetic and velocity fields as initial conditions, and remove the forcing. We find that if the initially supplied fields are too weak or too incoherent, they decay from the initial turbulent cascade faster than they can grow via the MRI. When the initially supplied fields are sufficient to allow MRI growth and sustenance, the saturated stresses, large-scale fields, and power spectra match those of the standard zero net flux MRI simulation with an initial large scale vertical field.

Key words: magnetic fields – MHD – dynamo – turbulence – accretion, accretion discs

1 INTRODUCTION

Magnetic fields are ubiquitous in turbulent astrophysical plasmas. While the mechanism of origin of large-scale ordered magnetic fields in these systems is a subtle business, more generic and less controversial is the amplification of total magnetic energy by the fluctuation or small-scale dynamo (SSD). Here, turbulence in a conducting plasma, with even a modest magnetic Reynolds number (R_m), leads to exponential growth of the field on the shortest eddy turn over time scales, which is usually much smaller than the age of the astrophysical system. The SSD is likely to be important for the early generation of magnetic fields in stars and galaxies/inter-stellar medium (ISM) (Sur et al. 2010; Gent et al. 2013; Bhat & Subramanian 2013). Such SSD generated fields would then be present in the plasma from stars or the ISM that source accretion disks.

In previous studies of the magneto-rotational instability (MRI) in shearing box models of accretion disks, the initial condition is typically an ordered *non-stochastic* field with net flux or zero-net flux. Following linear stability analysis, this kind of initial condition is the most natural to compare with minimalist analytic theory, but in reality one expects a more random field without necessarily much of a large-scale field. The question then arises as to whether and what kind of disorder and incoherence in the initial field can

still lead to MRI and field growth. Moreover, in general the source of an initial magnetic field itself, which could trigger MRI in a disk is not known. Initial fields in disks may be supplied externally and this may also be generated by SSD. Here, we explore this latter possibility, and the condition under which large-scale fields could grow and be sustained through MRI-driven turbulence initiated by SSD fields.

In the case of initial vertical fields of zero flux or net flux field, the MRI modes grow large-scale radial and azimuthal fields in the early linear growth phase (Bhat et al. 2016b; Ebrahimi & Blackman 2016) on orbital times scales eventually saturating nonlinearly to generate turbulence. It has been a long-standing topic of investigation to understand what determines the amplitude of the fields and stresses on MRI saturation, because this is thought to constrain the rate of angular momentum transport in accretion disks. The saturation amplitude of the stresses is not a constant across simulations but, for fixed resolution and box dimensions, depends on whether the initial field is of zero-net flux type or there is a uniform background field (Hawley et al. 1995; Fromang & Papaloizou 2007; Guan et al. 2009; Shi et al. 2016).

Here we investigate whether random fields (without a significant large-scale component) can seed the MRI, and whether the MRI sustains. Previous work using initially random fields (Hawley et al. 1996) had adopted a flat 1-D magnetic spectrum, and also with mostly large scale modes having $1 < k(L/2\pi) < 4$ and the

★ E-mail: pbhat@mit.edu

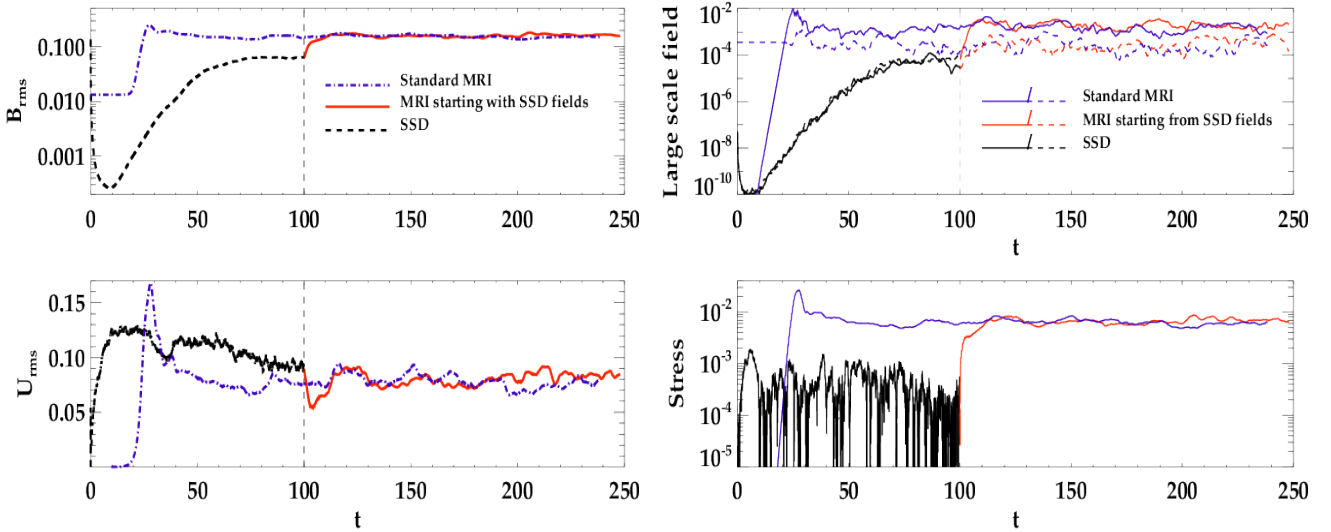


Figure 1. Evolution of B_{rms} and U_{rms} is shown in upper and lower left panels respectively for Run SSD, Run A0 and Run STD. Evolution of energy in large-scale magnetic fields and sum of Maxwell and Reynold stresses is shown in upper and lower right panels respectively for Run SSD, Run A0 and Run STD. The solid curves refer to x - y averaged fields while the dashed curves refer to y - z averaged fields.

field being 0 outside that interval. Such an initial field has a significant large scale component, (with the box scale field comparable to smaller scale fields), unlike the initial conditions we adopt below. In particular, we show that using small-scale fields (which by definition implies the absence of significant power at large scales) from a small-scale dynamo (SSD) as an initial condition, subsequent shear and rotation act to trigger MRI and as a result, sustains the turbulent fields even after the SSD forcing is turned off. We also discuss that the MRI fails to sustain when Gaussian random noise is instead used as an initial field. Note that Riols et al. (2013) generate an initial condition with random set of Fourier modes to study the transition to MRI turbulence, but with apparently large scale modes being energetically dominant. In our case, the Gaussian random initial fields are essentially noise-like with no large-scale component.

In section 2, we compare the sustained MRI turbulence with SSD initial condition against the case with zero net flux initial condition, with respect to the standard MRI signatures. Section 3 discusses the role of coherence in initial random magnetic fields for MRI to grow. The nature of MRI starting with SSD generated fields is investigated by spectral analysis in Section 4. We conclude in Section 5.

2 SUSTAINED MRI TURBULENCE WITH SSD INITIAL CONDITION

We perform shearing box simulations in a periodic box of $1 : 1 : 1$ aspect ratio using the PENCIL CODE¹. Most MRI simulations are of the resolution of 256^3 grid points and one fiducial run with 512^3 grid points. The model and the details of the simulation setup are the same as in Bhat et al. (2016b). The simulations are performed in two stages. First, to obtain the initial condition, we run a simulation of the SSD, without shear or rotation, with an imposed isotropic stochastic forcing in the momentum equation. Second, the velocity and magnetic fields from this small-scale dynamo simulation

(either from the kinematic or saturated stage), are introduced into a shearing box simulation as initial condition, with uniform shear $U_y = Sx$ (where S is the shearing rate) and rotation. The rotation is obtained by adding the Coriolis force term in the momentum equation, $2(\mathbf{\Omega} \times \mathbf{U})$, where $\mathbf{\Omega} = \Omega_0 \hat{z}$. In all of our runs, $S = -1.5$ and $\Omega_0 = 1$. Note that the stochastic forcing term used to obtain the SSD saturated state is subsequently turned off when the shearing box simulation begins with the SSD generated field as its initial condition. In principle, we could have run our SSD simulation in presence of shear, but then the properties of the SSD fields to be used as initial condition for MRI runs would vary as a function of the shearing rate. Thus we keep it simpler and the only free parameter which changes the properties of the SSD fields is the forcing scale.

In Fig. 1, we show the evolution of root mean square magnetic and velocity fields over time, for three runs of 512^3 resolution, (i) The SSD simulation run to saturation which is used to set the initial condition, called Run SSD (ii) the fiducial shearing box MRI simulation with initial fields from this SSD simulation, referred to as Run A0, starting at $t \sim 120$; and (iii) a standard MRI run starting with zero net flux of vertical large scale mode, Run STD. The magnetic Reynolds number is defined as $R_m = U_{\text{rms}} L / \eta$, where L is the size of the box and η is the microscopic resistivity and $R_m = 12000$ for Run SSD, while in Run STD and Run A0, the resulting R_m is 6000. The Prandtl number is $\text{Pr}_M = \nu / \eta$ and $\text{Pr}_M = 10$ for all the three runs. It can be seen that for Run A0 (shown in solid red lines), initial saturated SSD fields do not decay but grow and sustain due to MRI. The B_{rms} grows by a factor of ~ 2 to a value ~ 0.13 and U_{rms} decays by a factor of ~ 2 , saturating at a value of ~ 0.06 . Interestingly the saturation levels of both B_{rms} and U_{rms} match with those from Run STD. Fig. 1 also shows that the U_{rms} decays to a value which is smaller than the B_{rms} , thus going from a kinetically dominated system (SSD saturation phase) to a magnetically dominated system as would be the case for MRI turbulence.

We show the Reynolds and Maxwell stresses $\langle U_x U_y \rangle$ and $\langle B_x B_y \rangle$ for Run A0 compared to Run STD in the lower right panel of Fig. 1. The amplitude of the sum of the stresses in Run A0 is ~ 0.005 , which is the same as in Run STD. On the other hand, the

¹ <https://github.com/pencil-code> (Brandenburg 2003)

Run	k_f	k_{int}	B_{rms0}	U_{rms0}	$\gamma_{B_{rms}}$	Resolution
A0	1.5	7	0.06	0.090	0.0320	512 ³
A	1.5	7	0.06	0.095	0.0274	256 ³
B	5	14	0.06	0.09	0.0088	256 ³
C	10	23	0.05	0.08	0.0053	256 ³
D	1.5	14	0.02	0.12	0.0158	256 ³
E	1.5	15	0.008	0.12	0.0153	256 ³
F	1.5	15	0.004	0.12	0.0146	256 ³
G	1.5	15	0.002	0.12	-	256 ³
H	25	40	0.03	0.07	-	256 ³

Table 1. Summary of all runs: For each Run, the forcing scale k_f of the SSD run from which the initial condition is taken is specified, along with the k_{int} , the magnetic integral scale. Also shown are the initial magnetic and velocity field strengths, B_{rms0} and U_{rms0} , the growth rate of B_{rms} given by $\gamma_{B_{rms}}$ and the resolution.

stresses in Run SSD are very noisy and orders of magnitude below those of Run A0. A distinctive increase at $t \sim 120$ is seen, indicating the presence of MRI instability. We find that the Maxwell to Reynolds stress ratio in Run A0 is about 6.9, which matches well with the ratio ~ 6.7 estimated from the standard MRI simulation, Run STD (Brandenburg et al. 1995).

In the upper right panel of Fig. 1, we also show the evolution of planar averaged large-scale fields. The solid lines refer to x - y averaged fields and the dashed lines show the y - z averaged fields. The growth in the large-scale field in Run SSD is due to the low wavenumber tail of the magnetic power (peaked at large k) that results because the SSD eigenfunction grows self-similarly across all scales (Bhat & Subramanian 2013; Subramanian & Brandenburg 2014; Bhat et al. 2016a). However the saturation level is rather small at 10^{-5} . In the standard MRI simulation, the large-scale dynamo amplifies low wavenumber fields to a much higher amplitude $\sim 10^{-3}$ (Bhat et al. 2016b), and this also obtains in Run A0. In fact, from Fig. 1 top right panel, we see that again the amplitude of energy in large-scale fields from Run A0 matches with Run STD.

3 IMPORTANCE OF COHERENCE SCALES

3.1 SSD vs. Gaussian random noise as Initial Conditions

Unlike the case of the SSD initial conditions discussed in the previous section, we find that for a Gaussian random noise of even a large initial RMS field strength $B_{rms} \sim 0.1$ (finite perturbation), the field and velocity fluctuations decay in the shearing box run. This Gaussian random noise seed field was obtained by setting the vector potential to be normally distributed, uncorrelated random numbers in all meshpoints for all three components, which results in a spherical shell averaged magnetic power spectrum, \mathcal{E}_M , that increases with wave number k as $\mathcal{E}_M \sim k^4$. Note on the other hand, such Gaussian random noise field used as the initial condition in the Run SSD, does indeed lead to field growth. This is a particularly important point to note, because it immediately shows that while SSD mechanism is robust to any type of initial condition, MRI is sensitive to the nature of the initial field. Also we find that even when the criterion of providing finite (large amplitude) perturbations is satisfied as required for subcritical transition to turbulence, MRI modes still do not grow. We find another criterion that plays an important role namely the coherence scale of the initial fields. To understand this better, we examine the effect of varying magnetic integral scale (or the typical coherence scale) of

the initial fields on MRI. The magnetic integral length is defined as, $L_{int} = (\int (2\pi/k) \mathcal{E}_M dk) / (\int \mathcal{E}_M dk)$. The corresponding wavenumber is given by $k_{int} = 2\pi/L_{int}$.

In the SSD simulations, the forcing term in the momentum equation drives vortical motions localised around a wavenumber k_f , changing direction and phase at every time step (more details are given in Haugen et al. (2004)). Thus the turbulent outer scale of the velocity field is set at $k = k_f$. The growing magnetic fields in the SSD, peak near the resistive scales in the kinematic phase; but by saturation, the power shifts to larger scales closer to k_f (Bhat & Subramanian 2013). Therefore, we investigate the effect of increasing k_f (which increases k_{int}) during the SSD phase and how this influences subsequent growth and sustenance of MRI turbulence once the stochastic forcing is turned off.

3.2 Sensitivity of MRI to the k_f or k_{int} of the initial saturated SSD fields

Fig. 2 shows the time evolution of B_{rms} , U_{rms} and stresses in MRI simulations with initial SSD fields whose forcing wavenumbers were $k_f = 1.5, 5, 10$ and 25 , indicated by black, blue, red and green lines respectively. Runs with $k_f = 1.5, 5, 10$ and 25 are referred to as Run A, Run B, Run C and Run H respectively. The initial fields in the Runs A, B, C, H have the respective magnetic integral wavenumbers, $k_{int} = 7, 14, 23$ and 40 . The plots show that increasing k_f decreases the average growth rate and thus increases the time to reach saturation. The MRI modes which are triggered must be of larger wavenumber k for initial fields of larger k_f . One can perhaps understand this as follows: For an initially uniform vertical field B_0 , MRI unstable modes have a maximum growth rate for a wavenumber $k = k_{max} \propto \Omega/B_0$. One may roughly adopt a similar estimate for random fields, with now B_0 a measure of a suitably defined local coherent component of the field (such B_0 can be thought of as an average over a fixed scale between the different runs). For larger k_f , the magnetic power from the SSD is also peaked at a larger k , and for the same RMS value of the field, the B_0 would be smaller or k_{max} would be larger. These larger MRI unstable k modes are more affected by turbulent diffusion than lower k modes and thus incur smaller growth rates. In essence, we require that the MRI growth rate Ω for a given mode be larger than the corresponding turbulent diffusion rate, $(2\pi/3)k\nu(k)$, where $\nu(k)$ is the velocity at the wavenumber k , obtained from the kinetic power spectrum as $\sqrt{2kE_K(k)}$ i.e. $\Omega > (2\pi/3)k\nu(k)$, where k correspond to the fastest growing modes. We show in the right panel of Fig. 3, the curves $(2\pi/3)k\nu(k)$ from the initial velocity fields, for Runs A, B, C and H. We only make the assumption that the expected k_{max} is either equal to or larger than k_f . Only in the case of Run H, the growth of MRI modes is ineffective as the horizontal line of $\Omega = 1$ intersects the rate of turbulent diffusion already at about $k \sim 20$. The above interpretations also explain why an initial seed field of Gaussian random noise doesn't trigger MRI; namely that the coherence scale would be close to the grid resolution scale. Therefore, the presence of sufficiently coherent structures (effected here by small enough k_f) in SSD fields enables MRI growth, thus implying a minimum field coherence requirement.

3.3 Sensitivity of MRI to the strength of initial kinematic SSD fields

While the saturated SSD fields seem to be sufficiently coherent to trigger the MRI for a certain range of k_f we can also ask whether

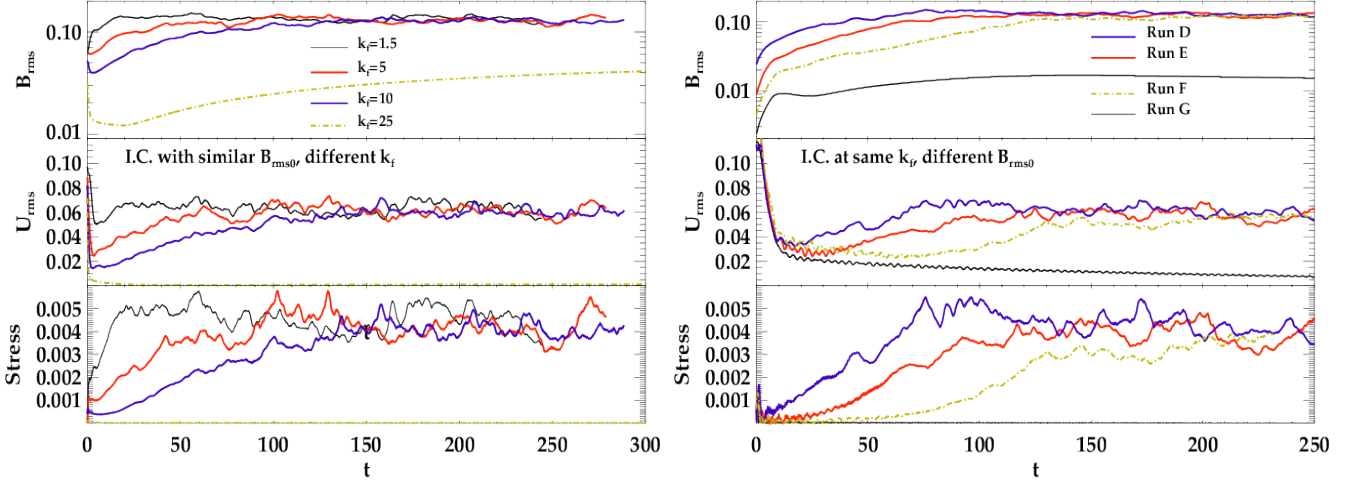


Figure 2. Evolution of B_{rms} and U_{rms} and stresses is shown in upper, middle and lower panels respectively for varying k_f in initial SSD fields in the left set and for varying $B_{\text{rms}0}$ in the right set. In the left set: the black, red, blue and green curves correspond to Run A, Run B, Run C and Run H where initial fields have $k_f = 1.5, 5, 10$ and 25 respectively with similar $B_{\text{rms}0}$ around $\sim 0.03 - 0.06$. In the right set: the blue, red, dashed green and black curves correspond to Run D, Run E, Run F and Run G where initial fields have $k_f = 1.5$, but decreasing $B_{\text{rms}0}$. We do not show the initial SSD phase here.

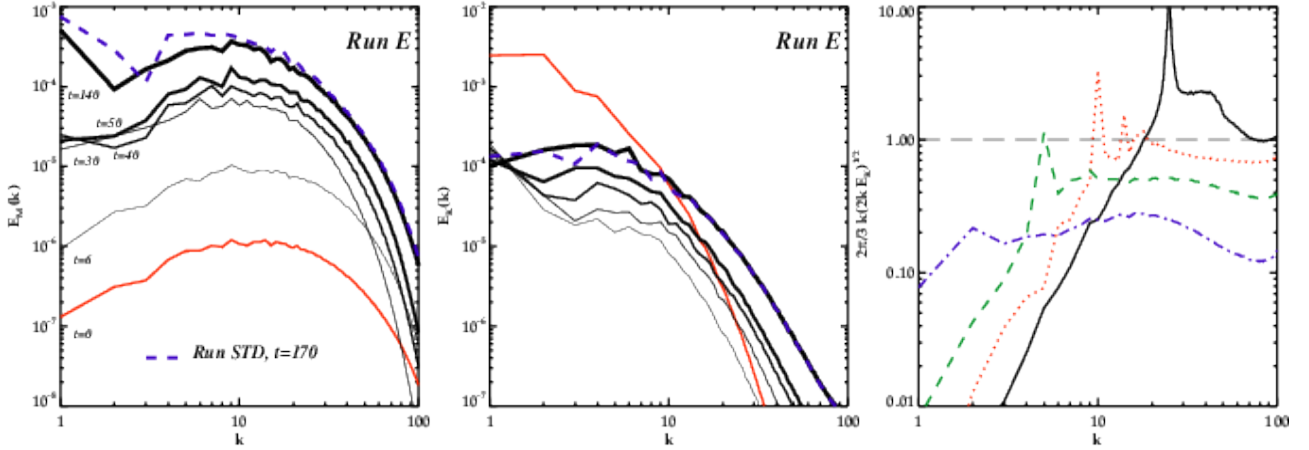


Figure 3. Evolution of magnetic power spectrum is shown in the left panel at times $t = 6, 30, 40, 50$ and 140 in solid black lines of increasing thickness. Similarly kinetic power spectrum is shown in the middle panel at times $t = 30, 40, 50, 60$ and 140 in solid black lines of increasing thickness. These are shown for Run E. The red curves are the initial spectra. And the dashed green curves correspond to the spectra from Run STD in saturation. In the right panel, the curves for rate of turbulent diffusion for the initial velocity field, $k v(k) = k \sqrt{2k E_K(k)}$ are shown for Run A (blue dash-dotted), Run B (green dashed), Run C (dotted) and Run H (black). The dashed horizontal line is MRI growth timescale $\Omega = 1$. Only Run H doesn't sustain as the turbulent diffusion rate is larger than the MRI growth rate.

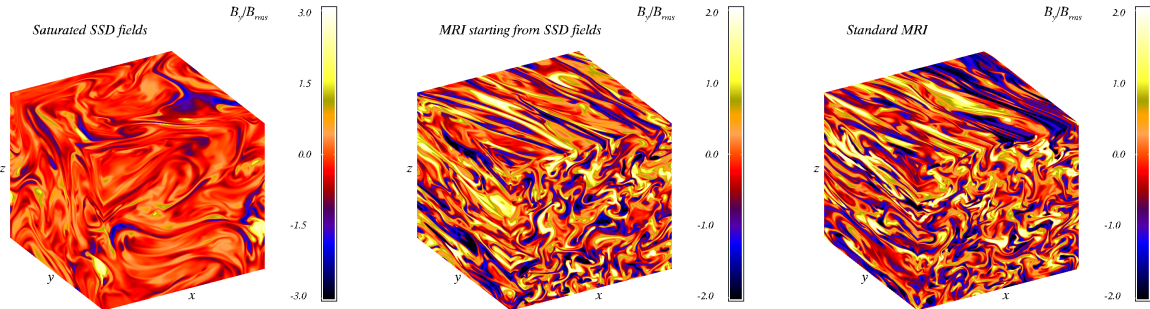


Figure 4. The azimuthal or B_y component of the magnetic fields are plotted for Run SSD, Run A0 and Run STD at high resolution of 512^3 in left, middle and right panels, from the saturated regimes.

SSD fields from just the kinematic regime are locally coherent enough to trigger MRI? We investigate this here using fields from the kinematic regime of SSD as initial condition for MRI.

The right panel of Fig. 2 shows the time evolution of total B_{rms} , U_{rms} and stresses in MRI simulations with SSD generated fields from the kinematic regime, of different initial field strengths $B_{\text{rms}0}$, but the same $k_f = 1.5$. The different curves are for $B_{\text{rms}0} \sim 0.02, 0.008, 0.004, 0.002$, shown in solid blue, solid red, dash-dotted green and solid black respectively; also referred as Run D, Run E, Run F and Run G. We find that MRI is triggered for initial SSD fields even from its kinematic regime. Again, here we find a trend of decreasing growth rate with decreasing $B_{\text{rms}0}$. Note that as we decrease the initial field, we also decrease the effective B_0 , and so increase the wavenumber of the fastest growing mode, where damping effects can slow down the growth.

Note that the magnetic field growth happens in two regimes, as seen from the evolution curves of B_{rms} and U_{rms} in the right panels of Fig. 2. At first, even as U_{rms} decays due to rapid turbulent cascade of the velocity, B_{rms} actually grows rapidly due to enhanced random shearing from these velocity flows. By "enhanced random shearing", we mean that even though the velocity field is decaying, the flow is still turbulent and there is a temporary SSD action enhanced by the uniform shear (Singh et al. 2016). But this gets subsequently overtaken by MRI action. Thereafter both B_{rms} and U_{rms} grow together due to MRI at the same rate up unto saturation. In the bottom-most curve in upper right panel of Fig. 2 in black, there is an initial increase of the magnetic field due to the random shearing, which however is not enough to trigger modes which are sufficiently large scale to compete with diffusion. Thus MRI modes do not grow in this particular run with $B_{\text{rms}0} \sim 0.002$. And while the velocity field (U_{rms}) decays further, the magnetic field, after the initial rapid growth due to random shearing, turns to saturate but continues to grow at a smaller rate due to the linear shearing action. However it eventually decays as it gets stretched out to resistive scales. We therefore show that the strength of total initial turbulent fields also has a critical role in triggering the MRI here.

Additionally, we considered the case in which SSD fields were allowed to decay (by removing the external forcing). Then such decayed (not fully) fields were used as initial condition for MRI. We again found that the MRI grows and saturates to the same amplitude as the other MRI growth cases. This is conceptually motivated by the possible circumstance whereby a disk forms from the collapse of a turbulent cloud or object whose forcing may not survive the transition. We have summarised the initial condition parameters for the different runs studied, in the Table 1. The growth rate of the B_{rms} calculated for each run is an average quantity given by $\gamma_{B_{\text{rms}}} = (\int_0^T dt d(\ln B_{\text{rms}})/dt)/T$, where T is the time taken to reach saturation.

4 SPECTRAL ANALYSIS OF MRI GROWTH

To understand how the power spectrum of the turbulent initial field evolves once the MRI takes over and whether there are any modal signatures akin to standard MRI linear phase, we study the initial SSD fields to MRI spectral evolution. Fig. 3 shows the evolution of magnetic and kinetic power spectra in Run E (corresponding to the solid red curves in right panel of Fig. 2) in the left and right panels respectively. The magnetic power spectrum, \mathcal{E}_M , first grows self-similarly from $t = 0$ to $t = 5$, due to enhanced random shearing action (similar to how the SSD spectrum grows c.f. Schekochihin et al. (2004), Haugen et al. (2004)). Then during $t = 30$ to $t = 50$,

the growth is due to linear MRI modes (when both B_{rms} and U_{rms} grow together). While growth is expected at all k , the MRI modes $k \sim 1-3$ do not grow much. Even if they did correspond to maximally growing modes, they would transfer all of their energy to larger wavenumbers. This indicates why the larger wavenumbers all grow by the same amount. A similar picture is seen for the kinetic spectra, \mathcal{E}_K , with little growth at lower wavenumbers ($k \sim 1-3$), but higher wavenumbers growing in unison. Note that between $t = 50$ to 140 , the small k modes become more and more prominent. In particular, the growth and maximum magnetic energy of small- k modes is around the same time (around $t = 140$) that the MRI stresses start to saturate (shown in Fig. 2 for run E). This is consistent with the notion that MRI saturation is connected to large-scale magnetic field generation (Ebrahimi et al. 2009). We therefore find that starting from more realistic turbulent SSD fields also sheds lights on the MRI saturation mechanism. Further analysis of MRI saturation remains for future work. Finally, the thickest solid black curves in both panels from the saturated regime are compared with the dashed curve at a similar time from the standard MRI run and they match well.

Note the peak at $k = 1$, which also indicates presence of large-scale fields (besides planar averaging). We find that the peak at $k = 1$ appears and disappears periodically, consistent with temporal cycles in the large-scale dynamo associated with planar averaged fields. The minimum requirement for large-scale MRI dynamo growth has been shown to be anisotropic fluctuations and shear to form a nonzero EMF (Ebrahimi & Blackman 2016). The form of EMF in terms of a mean field theory, such as incoherent alpha-shear or helicity flux source, is yet to be investigated (Vishniac & Brandenburg 1997; Vishniac & Cho 2001; Ebrahimi & Bhattacharjee 2014). Unlike runs in elongated shearing boxes, along with the peak at $k = 1$, there is a second peak around $k = 4-5$. Further investigation of the secondary peak is beyond the scope of the present paper.

Lastly, we show the azimuthal (B_y) component of magnetic fields from Run SSD, Run A0 and Run STD with a higher resolution of 512^3 in Fig. 4. For Run SSD, most of the box is orange indicating weaker small-scale fields. The scattered appearance of yellow or blue regions (both indicating higher magnitude fields) is due to the intermittency of the SSD. For Run A0 and Run STD, there are longer more coherent structures, particularly in the azimuthal direction, indicating the presence of large-scale fields. Also there are stronger small-scale fields as well, indicating higher contributions to Maxwell stresses compared to Run SSD. Note the characteristic vertical loopy structures (an MRI signature) in the x - z plane in both Run A0 and Run STD. Thus Run A0 and Run STD compare well indicating that such simulations (with zero net flux) are independent of the respective initial conditions.

5 CONCLUSIONS

We have shown via direct numerical simulations that the MRI can sustain MHD turbulence even when seeded with an initially random small-scale magnetic and velocity fields supplied by an SSD. In this case, the energy is strongly dominated by fields at small scales, implying that substantial power at low wave modes is not necessary for MRI growth

There is however, still a minimum strength and coherence required for this growth that is determined by a comparison between the turbulent diffusion time and MRI growth time near the wave number of maximum MRI growth. When the latter time scale is

shorter than the former, diffusion wins and the MRI does not grow. If the turbulent velocity forcing scale (a proxy for coherence) of initial fields is decreased or the field magnitude is decreased (by supplying an early unsaturated SSD state as an initial condition) then the fastest growing linear MRI mode moves to smaller scales where it has a harder time competing with diffusion. In short, if the initial coherence scales or strengths are too small, the MRI is quenched.

Generally, when the initial conditions are supplied by a saturated SSD, we find the conditions to be favorable for growth but when the initial field has a Gaussian random noise field the MRI fails to grow. The SSD is a natural initial condition as it is likely to be common in sufficiently conducting plasmas as in stars or the galactic ISM that feed accretion flows.

After the MRI takes over from the SSD supplied initial conditions, the saturated state of the magnetic and velocity fields in our simulations is essentially indistinguishable from that of the more commonly studied case of initial vertical fields of zero net flux. In particular the saturated amplitudes of the total magnetic and velocity fields (magnetic field being dominant), the accretion stresses, ratio of Maxwell to Reynolds stress, and the magnetic and kinetic power spectra are all very similar for the two aforementioned initial conditions.

Finally, we hypothesize that if only the SSD produced tangled magnetic field were supplied as an initial condition with the velocity removed, the turbulent decay rate would be lowered because the pre-removal $U_{rms} \geq V_A$. In the absence of an initial velocity, the minimum decay time is an Alfvén crossing time, which is itself the MRI growth time at k_{max} . Thus the aforementioned minimum field strength and coherence requirements are, if anything, less stringent when the velocity is absent. Further exploration of this hypothesis, and the understanding of the large-scale dynamo seen in these simulations would be of interest to explore in future work.

ACKNOWLEDGMENTS

We thank Jim Stone and Greg Hammett for thoughtful questions and discussions and Luca Comisso and Manasvi Lingam for some useful suggestions. PB and FE acknowledge grant support from DOE, DE-SC0012467. EB acknowledges support from grants HST-AR-13916.002, and NSF AST1515648. The computing resources were provided by Princeton Institute of Computational Science (PICSciE).

REFERENCES

- Bhat P., Subramanian K., 2013, *MNRAS*, **429**, 2469
- Bhat P., Subramanian K., Brandenburg A., 2016a, *MNRAS*, **461**, 240
- Bhat P., Ebrahimi F., Blackman E. G., 2016b, *MNRAS*, **462**, 818
- Brandenburg A., 2003, in Ferriz-Mas A., Núñez M., eds, *Advances in Non-linear Dynamos*. Taylor & Francis, London and New York, pp 269–344, doi:10.1201/9780203493137.ch9
- Brandenburg A., Nordlund A., Stein R. F., Torkelsson U., 1995, *ApJ*, **446**, 741
- Ebrahimi F., Bhattacharjee A., 2014, *Phys. Rev. Lett.*, **112**, 125003
- Ebrahimi F., Blackman E. G., 2016, *MNRAS*, **459**, 1422
- Ebrahimi F., Prager S. C., Schnack D. D., 2009, *Astrophys. J.*, **698**, 233
- Fromang S., Papaloizou J., 2007, *Astronomy & Astrophysics*, **476**, 1113
- Gent F. A., Shukurov A., Sarson G. R., Fletcher A., Mantere M. J., 2013, *MNRAS*, **430**, L40
- Guan X., Gammie C. F., Simon J. B., Johnson B. M., 2009, *ApJ*, **694**, 1010
- Haugen N. E., Brandenburg A., Dobler W., 2004, *PRE*, **70**, 016308
- Hawley J. F., Gammie C. F., Balbus S. A., 1995, *ApJ*, **440**, 742
- Hawley J. F., Gammie C. F., Balbus S. A., 1996, *ApJ*, **464**, 690
- Riols A., Rincon F., Cossu C., Lesur G., Longaretti P.-Y., Ogilvie G. I., Herauld J., 2013, *Journal of Fluid Mechanics*, **731**, 1
- Schekochihin A. A., Cowley S. C., Taylor S. F., Maron J. L., McWilliams J. C., 2004, *ApJ*, **612**, 276
- Shi J.-M., Stone J. M., Huang C. X., 2016, *MNRAS*, **456**, 2273
- Singh N. K., Rogachevskii I., Brandenburg A., 2016, preprint, (arXiv:1610.07215)
- Subramanian K., Brandenburg A., 2014, *MNRAS*, **445**, 2930
- Sur S., Schleicher D. R. G., Banerjee R., Federrath C., Klessen R. S., 2010, *ApJ*, **721**, L134
- Vishniac E. T., Brandenburg A., 1997, *ApJ*, **475**, 263
- Vishniac E. T., Cho J., 2001, *ApJ*, **550**, 752